

Multipole orders and Bragg diffraction patterns for the chain ferrate Na₂FeSe₂S. W. Lovesey^{1,2,*} and D. D. Khalyavin¹¹*ISIS Facility, STFC, Didcot, Oxfordshire OX11 0QX, United Kingdom*²*Diamond Light Source Ltd, Didcot, Oxfordshire OX11 0DE, United Kingdom*

(Received 19 August 2020; revised 7 March 2021; accepted 29 March 2021; published 19 April 2021)

Fundamental block and staggered orders of magnetic Fe multipoles in Na₂FeSe₂ are classified by their symmetry and magnetoelectric properties. Our minimal structure models incorporate ferromagnetic or antiferromagnetic coupling between chains, and they are not compatible with axial ferromagnetism. The ferrate salt is valued in studies of highly correlated electrons as the only iron selenide known to possess chainlike structural units hosting ferrous cations. Axial and polar (Dirac) multipoles are compulsory in the electronic structure since Fe ions exhibit enantiomorphic symmetry in the parent K₂ZnO₂-type compound. Calculated Bragg diffraction patterns for neutrons and x rays prove that the techniques can unlock individual contributions from both multipole types.

DOI: [10.1103/PhysRevB.103.134425](https://doi.org/10.1103/PhysRevB.103.134425)**I. INTRODUCTION**

This paper is a contribution to an ongoing quest for a deeper understanding of electronic properties of magnetic materials with captivating properties. We make use of symmetry-based techniques capable of unveiling fundamental aspects of a material without approximations that are inevitable in specific calculations, e.g., application of one of the many band structure methods. In our case, magnetic properties are formulated in terms of axial and polar multipoles that encapsulate electronic spin, orbital, and spatial degrees of freedom in the ground state. Motifs of multipoles are fully defined by magnetic space groups.

Axial multipole types represent conventional magnetism in the sense of its appearance in ichorlike hematite (α -Fe₂O₃) and famed lodestone worried and written about in Greek texts in 315 BC to Gilbert of Colchester, the father of magnetism, in the 16th century, to Dzyaloshinskii, in 1958 who gave a phenomenological theory of weak ferromagnetism. Polar (parity odd) magnetism is a relatively new discovery and intimately related to the property of electrically induced magnetization [magnetoelectric effect (ME)] measured for the first time in 1960 using a sample of Cr₂O₃. In this paper, we classify axial and polar multipole orders by their magnetic symmetry and ME response and predict their contribution to Bragg diffraction patterns available from illumination by beams of neutrons or x rays. Our results confirm that diffraction techniques can unlock many aspects of the magnetic properties of Na₂FeSe₂. For the moment, there is scant knowledge about the chalcogenide apart from its crystal structure because large samples are not yet available [1].

The chain ferrate salt Na₂FeSe₂ has aroused interest because it hosts ferrous cations and presents chainlike structural units [1,2]. These properties are not shared by iron-based superconductors that have been shown to possess

unusual magnetic orders [3,4], or TlFeS₂ [5] and selenide semiconductor TlFeSe₂ [6], which appear to contain quasi-one-dimensional units. The two-leg ladder selenide BaFe₂Se₃ hosts ferrous ions, however, and it supports a complicated magnetic order that remains to be fully resolved [7,8]. The variety of unusual magnetic phases presented by iron selenides is attributed to the interplay of spin, orbital, and lattice degrees of freedom, and orbital-lattice mechanisms are effective for the atomic configuration d^6 with its single electron outside a closed shell.

Electrical and magnetic properties of hematite and chromium sesquioxide (Cr₂O₃) serve as orientation to properties of block and staggered states of Na₂FeSe₂ delineated in Sec. III. Hematite and Cr₂O₃ have the centrosymmetric corundum structure with Fe and Cr ions in enantiomorphic sites (3, C₃), and likewise, the parent crystal structure of Na₂FeSe₂ is centrosymmetric with Fe ions in enantiomorphic sites. Furthermore, signatures of axial dipole moments along the trigonal axis are block and staggered for hematite and Cr₂O₃, respectively. The former is nonmagnetoelectric (high-temperature modification, 260–950 K, magnetic crystal class $2/m$), whereas Cr₂O₃ is a paradigm for the linear ME effect (magnetic crystal class $3'm'$). The ME effect allows a magnetic field to control electric polarization and an electric field to control magnetization by engaging magnetic degrees of freedom that violate both space-inversion and time-inversion symmetries.

Fundamental block and staggered states in Na₂FeSe₂, with ferromagnetic or antiferromagnetic couplings between chains, are here classified by a magnetic crystal class and a ME property. The compound is immediately interesting in the family of iron superconductors on account of a chainlike chemical structure, rather than ladderlike structure, and an atomic configuration that is not ferric. Two of 12 possible motifs in Na₂FeSe₂ are illustrated in Figs. 1 and 2, and all our classifications are listed in Table I. Axial dipoles are used in the labeling of motifs. Stabilization of a block motif, as in Fig. 1, is robust in a simulation of electronic structure [2].

*stephen.lovesey@stfc.ac.uk

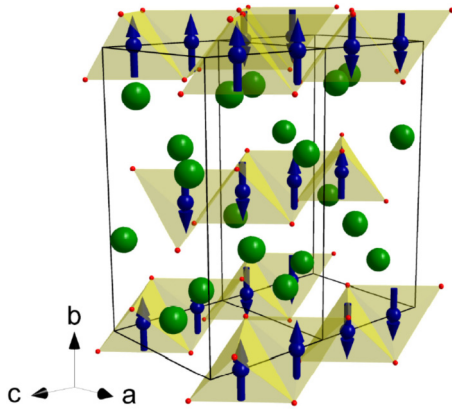


FIG. 1. Block state (I) in Na_2FeSe_2 with antiferromagnetic coupling between chains and axial dipole moments parallel to the b axis (shorthand b_β). Magnetic space group P_Cna2_1 (No. 33.151, BNS setting [29]), basis $(b, -a, 2c)$ and propagation vector $\mathbf{k} = (0, 0, \frac{1}{2})$.

While a block-type motif is well established in iron ladder compounds, it has yet to be observed in a chain compound. A staggered state of dipoles is depicted in Fig. 2. Alongside axial dipoles, one must consider anapoles. A toroidal anapole, more generally a Dirac dipole, is depicted in Fig. 3. Beyond dipoles (multipole rank 1) are axial and polar multipoles that are likely invisible in laboratory-based measurements. Our Bragg diffraction patterns for neutrons and x rays calculated for 12 possible motifs prove that contributions from the multipole types—axial and polar of rank 2 and higher—are open to observation and uniquely defined.

Neutron and x-ray Bragg diffraction methods are tried and tested mainstays in studies of magnetism since conciliation of crystal symmetry and magnetic phenomena strongly influences properties of a material. Neutrons are established as the first choice for the configuration of magnetic dipoles and distribution of magnetization, from Bragg diffraction patterns, and spectra of magnetic excitations, from inelastic scattering. For processes involving x-ray absorption and scattering, the content of the measured signal attributable to the magnetic

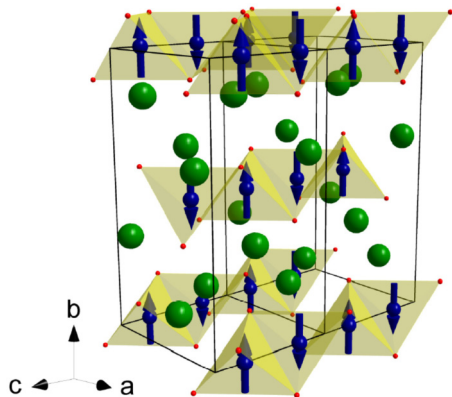


FIG. 2. Staggered state (II) with antiferromagnetic coupling between chains and axial dipole moments parallel to the b axis (shorthand b_β). Space group $Ib'am$ (No. 72.541 [29]), magnetic crystal class mmm' , basis $(-b, a, c)$ and propagation vector $\mathbf{k} = (0, 0, 0)$. A net anapole moment along the b axis is allowed.

TABLE I. Magnetic crystal classes are not compatible with ferromagnetism. Category (I) is polar ($mm21'$) and categories (II) and (III) are centrosymmetric (mmm' and $mmm1'$). Ferromagnetic and antiferromagnetic couplings between chains are labeled α and β , respectively. Magnetic space groups are specified in BNS setting [29]. All staggered states use site symmetry $22'2'$ for Fe ions with the dyad rotation operation 2 on the axis to which dipoles are aligned. Block states use site symmetry $2'_c$ for dipoles aligned along the a and b axes, and 2_c for alignment with the c axis. Shorthand b_β represents dipoles aligned along the b axis with antiferromagnetic coupling between chains, etc. Base vectors for each multipole order are listed.

(I) Block states: P_Cnm2 (No. 34.161) $c_\alpha (a, b, 2c)$; P_Cba2 (No. 32.139) $c_\beta (a, b, 2c)$: P_Cna2_1 (No. 33.151) a_α and $b_\beta (b, -a, 2c)$; a_β and $b_\alpha (a, b, 2c)$
(II) Staggered states: $Ib'am$ (No. 72.541) $a_\beta (a, b, c)$; $b_\beta (-b, a, c)$: $Iban'$ (No. 72.542) $c_\beta (a, -b, -c)$
(III) Staggered states: P_1bcm (No. 57.392) $a_\alpha (a, b, c)$; $b_\alpha (b, a, -c)$: P_1ccn (No. 56.376) $c_\alpha (a, b, c)$

properties of the sample, altogether, is pale and insignificant in its intensity compared to the intensity of contributions to the signal arising from electrical charge. At least for the moment, success in studying magnetic properties with x-ray beam techniques hinges on adopting a scheme to enhance the magnetic signal with respect to the charge signal. In absorption experiments, one exploits the sensitivity of the attenuation coefficient to the condition of the polarization in the primary beam, a so-called dichroic effect. A scheme for enhancing scattering signals is to tune the energy of the primary photon beam to the energy of a resonance in the magnetic ion of interest. Resonance-enhanced scattering, as it is sometimes called, has proved useful in a raft of studies of magnetic materials.

Development of a theory of magnetic neutron scattering has been an uneven ride. Prior to the Second World War, two Nobel Laureates created two different versions of the interaction operator, denoted here by \mathbf{Q} . Results by Bloch [9] and Schwinger [10] were eventually found in favor of

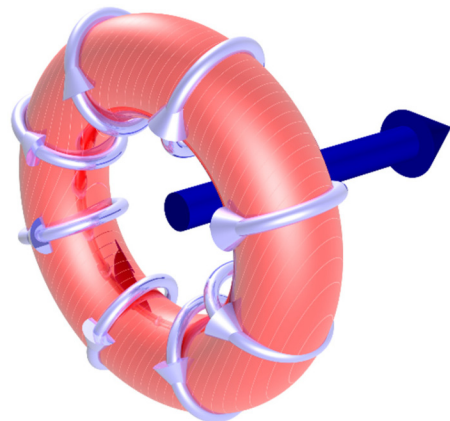


FIG. 3. Depiction of a toroidal (Dirac) dipole. Axial dipoles are used in Figs. 1 and 2.

Schwinger by Migdal [11]. The next big step came in 1953 when Trammell [12] reported the expectation value $\langle \mathbf{Q} \rangle$ suitable for the interpretation of Bragg diffraction patterns by rare earth and actinide materials with significant amounts of orbital magnetism. A calculation by Johnston [13] and Johnston and Rimmer [14] in 1966 turned in a seemingly different result for the same entity. Shortly thereafter, it was shown that the two results for $\langle \mathbf{Q} \rangle$ are indeed identical when Trammell's result for its orbital contribution is made gauge invariant [15]. In this communication, our method of working follows in the steps of Johnston's analysis [13,14,16].

Work by Hannon *et al.* and Luo *et al.* [17] on resonance-enhanced x-ray diffraction laid the foundation for studies of magnetic materials. Two papers provide the correct photon-electron mechanism and a theoretical development of the scattering amplitude in terms of axial magnetic multipoles.

Long-range magnetic order in a material is conventionally characterized by a motif of axial dipole moments. The dipoles in question are expectation values of the magnetic moment $\boldsymbol{\mu} = (2\mathbf{S} + \mathbf{L})$, where \mathbf{S} and \mathbf{L} are electronic spin and orbital operators, respectively. If dipole moments are zero, the motif is often labeled a hidden magnetic order or perhaps symmetry protected simply because it is not detected in observations conducted in the laboratory. While dipole moments might be forbidden by symmetry, the same ruling need not apply to expectation values of magnetic multipoles of higher rank, e.g., magnetic quadrupoles and octupoles might be different from zero. Fortunately, higher-rank axial and polar multipoles can be observed with beams of neutrons and x rays.

Properties of multipoles are ruled by 1 of the 122 magnetic point groups that delineate symmetry of a site in a magnetic ion. Multipoles mentioned in the previous paragraph are parity even (axial). Bulk properties of a magnetic crystal, e.g., the Kerr effect, are prescribed by the magnetic crystal class that is formed by the union of site symmetry (a point group) and translation symmetry in the motif. The Kerr effect can occur in the absence of a ferromagnetic motif of axial dipoles revealed by magnetic Bragg spots indexed on the chemical structure. If so, it arises from polar magnetism composed of Dirac multipoles. Such multipoles are products of time-odd electronic operators, \mathbf{S} or \mathbf{L} , and the time-even electric dipole operator \mathbf{R} , with final products magnetoelectric (time odd and parity odd). Expectation values of the spin anapole $\boldsymbol{\Omega}_S = \mathbf{S} \times \mathbf{R}$ or orbital anapole $\boldsymbol{\Omega}_L = (\mathbf{L} \times \mathbf{R} - \mathbf{R} \times \mathbf{L})$ may exist in this second scenario for magnetism, and a primary order parameter includes both axial and polar multipoles in the general case. Axial magnetism can be entirely forbidden, however, with allowed magnetism solely due to Dirac multipoles. A state of pure magnetic charge in a material is the assured outcome when magnetic ions occupy sites that possess inversions of space and time as conjugate symmetry operations. In such cases, anti-inversion $\bar{1}'$ is an element of site symmetry, and axial multipoles of any rank are forbidden. Of the 122 magnetic point groups, 21 contain anti-inversion $\bar{1}'$, and conventional, axial magnetism is absent. Magnetic charge, epitomized by a magnetic monopole, is notable by its absence in Maxwell's equations that unite electricity and magnetism. Artificially inserted in the equations, with symmetries of the electric and the magnetic field unchanged, magnetic charge is both time odd and parity odd, like Dirac's magnetic monopole. A Dirac

monopole ($\mathbf{S} \cdot \mathbf{R}$) can contribute to x-ray scattering, but it is forbidden by symmetry from contributing to neutron scattering. A monopole using \mathbf{L} does not exist because \mathbf{L} and \mathbf{R} are orthogonal operators and $(\mathbf{L} \cdot \mathbf{R}) = 0$.

II. MATERIAL PROPERTIES

Na_2FeSe_2 is composed of chainlike structural units in an I-centered orthorhombic K_2ZnO_2 -type structure, with symmetry mmm (D_{2h}) [1]. Edge-sharing (FeSe_4) tetrahedra occupy the chemical structure *Ibam* (No. 72) with Fe (4a) at $\{(0, 0, \frac{1}{4}), (0, 0, \frac{3}{4})\}$. Cations Fe^{2+} are likely to have the high-spin 5D , $J = 4$, $3d^6$ atomic configuration. Atomic $3d$ states of a ferrous ion and the K_2ZnO_2 -type crystal structure are nicely illustrated in fig. 8 of Ref. [1].

There is growing conviction that Na_2FeSe_2 possesses magnetic states with signatures $\downarrow\downarrow\uparrow\uparrow\downarrow\downarrow$ and $\downarrow\uparrow\downarrow\uparrow$ for dipoles situated on a chain [1,2]. Yet no mention to date of the inescapable fact that magnetic dipoles are axial moments and anapoles. For ferrous ions (Fe^{2+}) in the parent compound occupy enantiomorphic sites (222 (D_2) point symmetry), and both axial and Dirac magnetic multipoles are present with the onset of magnetic order.

III. MODEL STRUCTURES

Multipole orders in Na_2FeSe_2 are derived from dipole moments parallel to crystal axes. Bulk axial ferromagnetism is absent. Twelve orders in the minimal model are classified by a magnetic crystal class and a ME property, which is a principal result of our study. (I) Polar $mm21'$ with time reversal $1'$ permits a spontaneous dielectric polarization and a nonlinear ME effect; (II) centrosymmetric mmm' with anti-inversion $\bar{1}'$ and a linear ME effect akin to the magnetic state of Cr_2O_3 ; (III) centrosymmetric $mmm1'$ with all three inversions $\bar{1}, 1', \bar{1}'$, and any kind of ME is prohibited. Categories (I) and (III) are antiferromagnetic motifs with nontrivial Bravais lattices defined by propagation vectors $\mathbf{k} = (0, 0, \frac{1}{2})$ and $\mathbf{k} = (1, 1, 1)$, respectively. A ferroelectric state allowed in (I) is realized in boracites, for example. Category (II) possesses a trivial antiferromagnetic motif with $\mathbf{k} = (0, 0, 0)$. All six block states $\downarrow\uparrow\uparrow\downarrow\downarrow$ under consideration belong to (I), while staggered states $\downarrow\uparrow\downarrow\uparrow$ are divided between (II) or (III), the difference being antiferromagnetic (II) or ferromagnetic (III) coupling between chains. Magnetic space groups for the multipole orders are gathered in Table I.

IV. BRAGG DIFFRACTION PATTERNS

A structure factor for diffraction is $\Psi_Q^K = [\exp(i\boldsymbol{\kappa} \cdot \mathbf{d}) \langle O_Q^K \rangle_{\mathbf{d}}]$, where the Bragg wave vector $\boldsymbol{\kappa}$ is defined by integer Miller indices (h, k, l), and the implied sum in Ψ_Q^K is over all Fe sites \mathbf{d} in a magnetic unit cell. An electronic multipole $\langle O_Q^K \rangle$ of rank K with projections $-K \leq Q \leq K$ possesses discrete symmetries [Cartesian and spherical components of a dipole $\mathbf{R} = (x, y, z)$ are related by $x = (R_{-1} - R_{+1})/\sqrt{2}$, $y = i(R_{-1} + R_{+1})/\sqrt{2}$, $z = R_0$]. In the case of magnetic diffraction, a multipole is time odd ($\sigma_\theta = -1$) and parity even ($\sigma_\pi = +1$, axial) or parity odd ($\sigma_\pi = -1$, Dirac multipole). Bulk signals are proportional to

Ψ_Q^K evaluated for $\kappa = 0$, and examples include net electric dipole and anapole motifs allowed in categories (I) and (II), respectively. Structure factors for magnetic multipoles in category (I) are zero for Miller index l even irrespective of their parity.

First, we consider diffraction by six multipole orders in category (I). Following notation used in Table I, ferromagnetic (antiferromagnetic) coupling between chains is labeled $\alpha(\beta)$. Corresponding dipoles along the a and b axes are denoted by shorthand $a_\alpha(a_\beta)$ and $b_\alpha(b_\beta)$. Four block states conforming to these dipole motifs all belong to space group P_Cna2_1 (No. 33.151 BNS), and b_β is depicted in Fig. 1. The corresponding structure factor is

$$\Psi_Q^K(33.151) \propto [1 + (-1)^l \sigma_\theta] [\langle O_Q^K \rangle + (-1)^{h+k} (-1)^K \sigma_\theta \times \sigma_\pi \langle O_{-Q}^K \rangle]. \quad (1)$$

Projections Q are odd, and $\langle O_{-Q}^K \rangle = (-1)^Q \langle O_Q^K \rangle^* = -\langle O_Q^K \rangle^*$. Base vectors $(a, b, 2c)$ and $(b, -a, 2c)$, with site symmetry $2'_c$, apply to block states using a_β, b_α and a_α, b_β , respectively. Symmetry constraints mentioned apply to axial and Dirac multipoles, e.g., Eq. (1) applies to axial moments and anapoles on taking $K = 1$ and the appropriate values of time and parity signatures. The time signature is included in Eq. (1) since our electronic structure factors describe both Thomson scattering and resonance enhanced diffraction of x rays [22], in addition to magnetic neutron diffraction ($\sigma_\theta = -1$). The selection rule l odd applies for magnetic diffraction, and it corresponds to a propagation vector $\mathbf{k} = (0, 0, \frac{1}{2})$. Referred to Miller indices for the parent structure (H_o, K_o, L_o) and base vectors $(a, b, 2c)$, it follows that $h = H_o, k = K_o, l = 2L_o$ with L_o half-integer. Diffraction amplitudes for axial dipoles and anapoles in the basal plane are 90° out of phase, and corresponding intensities add. Moreover, the two dipoles are orthogonal, and relative contributions are changed by the choice of Miller indices h and k .

The structure factor Eq. (1) applies to the block state c_α described by P_Cnn2 (No. 34.161) with base vectors $(a, b, 2c)$ and site symmetry 2_c . Thus, projections Q are even integers. In consequence, dipoles ($K = 1, Q = 0$) obey strict selection rules $h + k$ even (axial) or $h + k$ odd (anapole). Selection rules for diffraction by the block state using c_β are derived from P_Cba2 (No. 32.139). Base vectors and site symmetry for c_α and c_β are the same. However, σ_θ does not occur as a coefficient of $\langle O_{-Q}^K \rangle$ in Ψ_Q^K (32.139), which is otherwise the same as Eq. (1), and dipole selection rules are the reverse of those already mentioned for Ψ_Q^K (34.161).

Turning to staggered multipole orders (II) and (III), the electronic structure factor

$$\Psi_Q^K(57.392) \propto \langle O_Q^K \rangle [1 + (-1)^l \sigma_\theta \sigma_\pi] [1 + (-1)^{h+k+l} \sigma_\theta], \quad (2)$$

with Q odd is appropriate for the staggered state using dipoles a_α and b_α . Site symmetry $2'2'$ applies with base vectors (a, b, c) and $(b, a, -c)$ for a_α and b_α , respectively. I-centering is violated by multipole order (III) with propagation vector $\mathbf{k} = (1, 1, 1)$, and the selection rule on l distinguishes between diffraction by axial ($\sigma_\theta \sigma_\pi = -1$) and Dirac ($\sigma_\theta \sigma_\pi = +1$) types. The latter feature is common to all staggered states under consideration. I-centering is restored in category

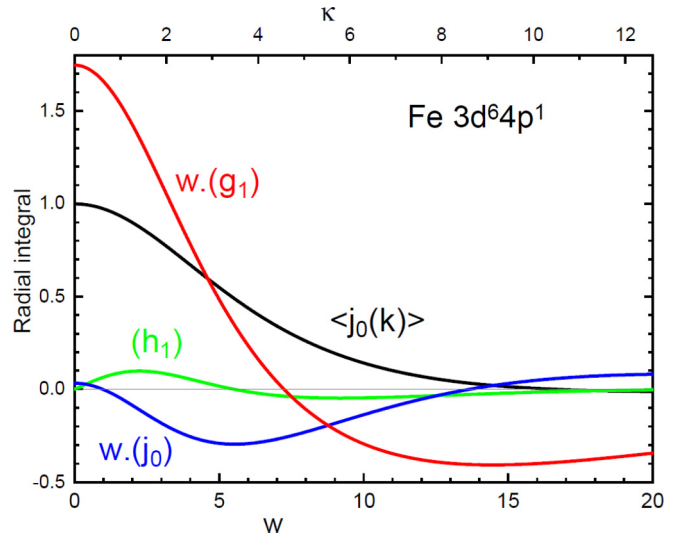


FIG. 4. Radial integrals for neutron diffraction by magnetic dipoles calculated using Cowan's atomic code [20]. $\langle j_0(\kappa) \rangle$ in black for equivalent electrons $3d^6$ accompanies the magnetic moment. Atomic configuration $\text{Fe}(3d^6)\text{-Fe}(4p^1)$ is used for anapole radial integrals: (red) $[w(g_1)]$; (green) (h_1) ; (blue) $[w(j_0)]$, where the dimensionless wave vector $w = 3a_o\kappa$ and a_o is the Bohr radius. $\kappa = [(4\pi/\lambda) \sin(\theta)]$, where λ and θ are the neutron wavelength and Bragg angle, respectively, cf. Fig. 5. Both (g_1) and (j_0) diverge in the limit $w \rightarrow 0$, and values displayed are multiplied by w . Integrals $(g_1), (h_1), (j_0)$ accompany dipoles $i\mathbf{R}, \mathbf{\Omega}_s, \mathbf{\Omega}_L$, respectively, in the Dirac dipole \mathbf{D} .

(II) using a_β and b_β described by $\Psi_Q^K(72.541)$, which is the same as Eq. (2) apart from replacement of the antitranslation selection rule by I-centering. Base vectors are (a, b, c) and $(-b, a, c)$ with site symmetry $2'2'$ for a_β and b_β , respectively, and a motif is depicted in Fig. 2. A net anapole moment is allowed, i.e., Ψ_Q^K evaluated for $\kappa = 0$ and $\sigma_\theta \sigma_\pi = +1$ can be different from zero. Staggered states using dipoles aligned with the c axis have even projections Q from site symmetry $2'2'$. Implementing this site symmetry, we find $\Psi_Q^K(56.376) = \Psi_Q^K(57.392)$ for c_α and base vectors (a, b, c) . Finally, the staggered state using c_β belongs to multipole order (II) described by $\Psi_Q^K(72.542)$ with base vectors $(a, -b, -c)$.

Necessary conditions on Miller indices for diffraction to occur include: (I) $(-1)^l = \sigma_\theta$; (II) $(-1)^l = \sigma_\theta \sigma_\pi$; (III) $(-1)^l = \sigma_\theta \sigma_\pi$ with $(-1)^{h+k} = \sigma_\pi$. The individual conditions are consistent with an absence of bulk axial ferromagnetism.

V. NEUTRON DIFFRACTION

Interaction between neutrons and unpaired electrons is simple to formulate for small values of the scattering wave vector κ [18]. Most authors analyze experimental data for elastic (Bragg) and inelastic scattering with an approximation to the interaction operator \mathbf{Q} proportional to $\{\boldsymbol{\mu} \cdot (j_0(\kappa))\}$, where the radial integral $\langle j_0(\kappa) \rangle$ is displayed in Fig. 4 [19]. An improved approximation $\{\langle \mathbf{J} \rangle [g(j_0(\kappa)) + (2-g)\langle j_2(\kappa) \rangle]\}$, where g is the Landé splitting factor, and the two radial integrals satisfy $\langle j_0(0) \rangle = 1$ and $\langle j_2(0) \rangle = 0$, is more appropriate for the analysis of Bragg diffraction patterns composed

of many spots extending to large κ . Beyond dipoles, the quadrupole ($K = 2$) proportional to $\langle j_2(\kappa) \rangle$ is zero for states in a J manifold, while the octupole ($K = 3$) has a form factor that includes $\langle j_4(\kappa) \rangle$. It is compulsory to add Dirac multipoles to the foregoing axial multipoles when magnetic ions occupy acentric sites. The Dirac dipole \mathbf{D} contributes a term $\{i(\boldsymbol{\kappa} \times \mathbf{D})/\kappa\}$ to \mathbf{Q} . The dipole is a sum of a spin anapole $\boldsymbol{\Omega}_S$, orbital (toroidal) anapole $\boldsymbol{\Omega}_L$ and $i\mathbf{R}$. Radial integrals that accompany each dipole are displayed in Fig. 4 [20]. Figure 3 depicts a toroidal (Dirac) dipole. Dirac quadrupoles account for magnetic neutron diffraction by the pseudogap phases of ceramic superconductors YBCO and Hg1201 [21].

Let us consider an antiferromagnetic state with axial dipoles and anapoles aligned along the crystal c axis. Our notation for the multipole order is c_β and staggered (II). In this case, ferrous ions occupy sites $4a$ in magnetic space group $Ibam'$ (No. 72.542) with base vectors $(a, -b, -c)$. Projections Q of multipoles $\langle O_Q^K \rangle$, both axial and polar, are restricted to even values by virtue of a rotation element 2_c in site symmetry $2'2'2$. Dyads parallel to the a and b axes are therefore equivalent, and symmetry $2'_a$ demands $\langle O_Q^K \rangle = (-1)^K \sigma_\theta \langle O_{-Q}^K \rangle = (-1)^{K+1} \langle O_Q^K \rangle^*$. The appropriate electronic structure factor is derived from Eq. (2) by installing I-centering, i.e., Miller indices $h + k + l$ even. Index l is even (odd) for parity-odd (even) multipoles, meaning Ψ_Q^K evaluated for $h = k = l = 0$ can be different from zero for $\sigma_\theta \sigma_\pi = +1$. Specifically, a net anapole moment parallel to the c axis is allowed by symmetry.

Assuming atomic states are drawn from a J manifold, parity-even multipoles $\langle T_Q^K \rangle$ have an odd rank [18]. Restricting attention to dipoles and octupoles,

$$\begin{aligned} \langle \mathbf{Q}^{(+)} \rangle_a &\approx \sqrt{210} p_a p_c \left[\langle T^{3+2} \rangle - \sqrt{\left(\frac{3}{10}\right)} \langle T^3_0 \rangle \right], \\ \langle \mathbf{Q}^{(+)} \rangle_b &\approx -\sqrt{210} p_b p_c \left[\langle T^{3+2} \rangle + \sqrt{\left(\frac{3}{10}\right)} \langle T^3_0 \rangle \right], \\ \langle \mathbf{Q}^{(+)} \rangle_c &\approx 6 \langle T^1_c \rangle, \end{aligned} \quad (3)$$

where the superscript denotes $\sigma_\pi = +1$. The amplitude for magnetic diffraction $\langle \mathbf{Q}_\perp \rangle = \{\mathbf{p} \times ((\mathbf{Q}) \times \mathbf{p})\}$ with a unit vector $\mathbf{p} = \boldsymbol{\kappa}/\kappa$, and $p_a \propto h$, $p_b \propto -k$, $p_c \propto -l$ in the present case. Results in Eq. (3) can be derived from published universal expressions [18]. A useful approximation for the dipole

$$\langle \mathbf{T}^1 \rangle \approx \left(\frac{1}{3}\right) \{2\langle \mathbf{S} \rangle \langle j_0(\kappa) \rangle + \langle \mathbf{L} \rangle [\langle j_0(\kappa) \rangle + \langle j_2(\kappa) \rangle]\}, \quad (4)$$

is consistent with a previously quoted estimate. Octupoles in Eq. (3) are purely real and proportional to $[\langle j_2(\kappa) \rangle - (\frac{4}{3})\langle j_4(\kappa) \rangle]$ for $3d^6$. Powder diffraction intensity is derived from the general result

$$\begin{aligned} &\left(\frac{1}{4}\pi\right) \int d\widehat{\boldsymbol{\kappa}} \{ \langle \mathbf{Q}_\perp^{(+)} \rangle \cdot \langle \mathbf{Q}_\perp^{(+)} \rangle \} \\ &= \sum_{K,Q} \left[\frac{3}{(2K+1)} \right] |\langle T^{K,Q} \rangle|^2 + \sum_{K',Q'} \left[\frac{3}{(K'+1)} \right] |\langle T^{K',Q'} \rangle|^2, \end{aligned} \quad (5)$$

with K even ($= 2, \dots, 2l_o$) and K' odd ($= 1, 3, \dots, 2l_o + 1$), where l_o is the orbital angular momentum of the atomic shell.

A leading-order approximation to the parity-odd amplitude with Miller index l even is

$$\begin{aligned} \langle \mathbf{Q}_\perp^{(-)} \rangle_a &\approx 4i p_b \langle \mathbf{D} \rangle_c, \quad \langle \mathbf{Q}_\perp^{(-)} \rangle_b \approx -4i p_a \langle \mathbf{D} \rangle_c, \\ \langle \mathbf{Q}_\perp^{(-)} \rangle_c &\approx -\left(\frac{24}{\sqrt{5}}\right) p_a p_b p_c \langle H^2_{+2} \rangle. \end{aligned} \quad (6)$$

The orbital-spin quadrupole $\langle H^2_{+2} \rangle$ is purely imaginary and proportional to the radial integral (h_1) displayed in Fig. 4, which also accompanies the spin anapole in the Dirac dipole.

We choose the electronic structure factor Eq. (1) to illustrate diffraction by a block state in category (I). Site symmetry $2'_c$ demands that projections Q are odd. Miller index l is odd, and $h + k$ is taken to be even. Restricting attention to dipoles, we find

$$\begin{aligned} \langle \mathbf{Q}_\perp \rangle_a &\approx -p_a p_b \langle \mathbf{Q}^{(+)} \rangle_b, \\ \langle \mathbf{Q}_\perp \rangle_b &\approx -[1 - p_b^2] \langle \mathbf{Q}^{(+)} \rangle_b + 4i p_c \langle \mathbf{D} \rangle_a, \\ \langle \mathbf{Q}_\perp \rangle_c &\approx -p_b p_c \langle \mathbf{Q}^{(+)} \rangle_b - 4i p_b \langle \mathbf{D} \rangle_a, \quad \text{with} \\ \langle \mathbf{Q}^{(+)} \rangle_b &\approx -6 \langle \mathbf{T}^1 \rangle_b. \end{aligned} \quad (7)$$

Components of axial and polar dipoles are here parallel to the b and a axes, respectively. The situation is the reverse for $h + k$ odd.

VI. X-RAY DIFFRACTION

Studies of various materials using resonant x-ray Bragg diffraction, accompanied by supporting calculations, are reported in Refs. [22,23]. The photon scattering amplitude derived from quantum electrodynamics is developed in the small quantity E/mc^2 , where E is the primary energy ($mc^2 \approx 0.511$ MeV). At the second level of smallness in this quantity, the amplitude contains resonant processes that may dominate all other contributions should E match an atomic resonance Δ . Assuming also that virtual intermediate states are spherically symmetric, the scattering amplitude $\approx \{F_{\mu\nu}/(E - \Delta + i\Gamma/2)\}$ in the region of the resonance, where Γ is the total width of the resonance. The numerator $F_{\mu\nu}$ is a unit-cell structure factor for Bragg diffraction in the scattering channel with primary (secondary) polarization $\nu(\mu)$. In keeping with convention, σ denotes polarization normal to the plane of scattering, and π denotes polarization within the plane of scattering. The Bragg angle is denoted by θ , and the primary beam is deflected through an angle 2θ . Figure 5 depicts polarization states, wave vectors, and the Bragg condition. Our unit-cell structure factors include a dependence on the rotation of the crystal through an angle ψ around the Bragg wave vector $\boldsymbol{\kappa}$.

Parity-even and parity-odd x-ray absorption events occur at different energies. Axial multipoles (t_Q^K) are observed in Bragg diffraction enhanced by an electric dipole-electric dipole ($E1$ - $E1$) event, for example, while Dirac multipoles (G_Q^K) contribute to diffraction enhanced by an electric dipole-electric quadrupole event ($E1$ - $E2$) [22,23]. Valence states $3d$ and $4p$ are engaged by absorption at $2p$ states (L edges). In so far as hydrogenic forms of radial wave functions are

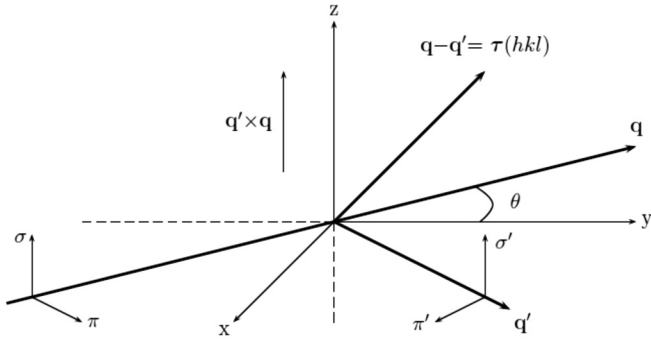


FIG. 5. X-ray diffraction. Primary (σ , π) and secondary (σ' , π') states of polarization. Corresponding wave vectors \mathbf{q} and \mathbf{q}' subtend an angle 2θ , and the Bragg condition is met when $\boldsymbol{\kappa} = \mathbf{q} - \mathbf{q}'$ coincides with a reciprocal lattice vector $\boldsymbol{\tau}(hkl)$. Cell edges of a crystal and depicted Cartesian coordinates (x , y , z) coincide in the nominal setting of the crystal.

appropriate for the photo-ejected $2p$ electron and empty $3d$ and $4p$ valence states, radial integrals for $E1$ - $E2$ and $E1$ - $E1$ events are in a ratio $\langle 2p|R^2|4p\rangle/\langle 2p|R|3d\rangle = -1.66a_0/Z_o$, where Z_o is the effective core charge seen by the jumping electron and a_0 is the Bohr radius. Sum rules for L_2 and L_3 edges $\langle \mathbf{t}^1 \rangle_{L_3} + \langle \mathbf{t}^1 \rangle_{L_2} = -\langle \mathbf{L} \rangle_{3d}/(10\sqrt{2})$ [24], and $\langle \mathbf{t}^2 \rangle_{L_3} + \langle \mathbf{t}^2 \rangle_{L_2} = \langle \{\mathbf{L} \otimes \mathbf{L}\}^2 \rangle_{3d}/60$, with $\langle \mathbf{L} \otimes \mathbf{L} \rangle_0^2 = [3(L_z)^2 - L(L+1)]$ for the diagonal element of the tensor product, demonstrate that contributions by $3d$ spin degrees of freedom are equal and opposite at the two edges (energies of iron L_3 , L_2 , and K edges ≈ 0.708 , 0.721 , and 7.112 keV, respectively). The sum rule for anapoles is $\langle \mathbf{G}^1 \rangle_{L_3} + \langle \mathbf{G}^1 \rangle_{L_2} = -\langle \mathbf{R} \times \boldsymbol{\mu} \rangle_{3d}/(2\sqrt{2})$.

The polar property of magnetic crystal class $mm21'$ for category (I) is manifest in the result $\Psi_0^1(\boldsymbol{\kappa} = 0) = 4\langle U_0^1 \rangle$, where $\langle U^1 \rangle$ is a time-even polar dipole akin to the displacement $\langle \mathbf{R} \rangle$. Also, $\Psi_0^2(\boldsymbol{\kappa} = 0) = 0$ indicates a null value of the natural circular dichroic signal. Bragg diffraction patterns that violate I-centering are of some interest, for they are created by angular anisotropy in the charge density as in Templeton-Templeton scattering [25]. Consider nonmagnetic diffraction

$$F_{\sigma'-\sigma} = -\left(\frac{4}{5}\right)\sqrt{\left(\frac{2}{3}\right)}\Re \cos(\theta)\{\sin(\Psi)[3\langle G_{+1}^1 \rangle' + \sqrt{5}\langle G_{+1}^2 \rangle'' - \langle G_{+1}^3 \rangle'] + \sqrt{15}\sin(3\Psi)\langle G_{+3}^3 \rangle'\},$$

$$F_{\pi'-\sigma} = -\left(\frac{2}{5}\right)\sqrt{\left(\frac{2}{3}\right)}\Re \sin(2\theta)\{\cos(\Psi)[-3\langle G_{+1}^1 \rangle' + 2\sqrt{5}\langle G_{+1}^2 \rangle'' + \langle G_{+1}^3 \rangle'] + \sqrt{15}\cos(3\Psi)\langle G_{+3}^3 \rangle'\}.$$

Note the identity $\langle \mathbf{G}^1 \rangle_a = -\sqrt{2}\langle G_{+1}^1 \rangle'$. A magnetic monopole (G_0^0) allowed in block states c_α and c_β (space groups Nos. 34.161 and 32.139 in Table I) can contribute to diffraction enhanced by an electric dipole-magnetic dipole ($E1$ - $M1$) event. By its very nature, the monopole contribution is independent of the azimuthal angle, which makes for challenging identification [26].

VII. DISCUSSION

We enumerated motifs of magnetic multipoles in the ferrate salt Na_2FeSe_2 . With chainlike structural units and ferrous cations, it is a unique iron selenide material [1]. In terms of

using $h+k$ odd, with l even, for block states as in Eq. (1). Enhancement by an $E1$ - $E2$ event reveals polar quadrupoles and octupoles, $\langle U_{+2}^2 \rangle$, $\langle U_{+2}^2 \rangle'$, $\langle U_{+2}^3 \rangle''$, where real and imaginary parts obey the phase in $\langle \mathbf{U}^K \rangle' + i\langle \mathbf{U}^K \rangle''$. The unit-cell structure factor for Bragg reflections $(h, 0, 0)$ with h odd in the $\sigma' - \sigma$ channel is found to be

$$F_{\sigma'-\sigma} = -2\sqrt{\left(\frac{2}{15}\right)}\Re \sin(\theta)\sin(2\Psi)\left[\sqrt{\left(\frac{3}{2}\right)}\langle U_{+2}^2 \rangle + \langle U_{+2}^2 \rangle' + 2\sqrt{2}\langle U_{+2}^3 \rangle''\right],$$

where the dimensionless quantity

$$\Re = \left\{ \frac{\alpha E}{2a_0 R_\infty} \right\} \left[\frac{\langle 2p|R^2|4p\rangle}{\langle 2p|R|3d\rangle} \right],$$

values an $E1$ - $E2$ structure factor relative to $E1$ - $E1$ ($R_\infty \approx 13.6$ eV, and α is the fine structure constant). The origin of the azimuthal angle places the crystal c axis normal to the plane of scattering depicted in Fig. 5. In the rotated channel of polarization, the ψ dependence of $F_{\pi'-\sigma}$ is $\cos(2\psi)$, while its dependence on θ is different for each of the three multipoles.

After this diversion on diffraction by time-even multipoles, we return to magnetic scattering and explore the electronic structure factor Eq. (1). Equation (7) with axial and polar multipoles is a corresponding neutron diffraction amplitude. Bulk signals are zero, including magnetochiral and nonreciprocal linear dichroic signals, because l is required odd. Axial magnetic dipoles contribute to x-ray diffraction in the $\pi'\sigma$ channel. For a Bragg wave vector $(0, 0, l)$ with l odd and diffraction enhanced by an $E1$ - $E1$ event, $F_{\pi'-\sigma}$ is proportional to $\langle \mathbf{t}^1 \rangle_b \cos(\theta) \cos(\psi)$. By comparison, diffraction enhanced by an $E1$ - $E2$ event reveals the a component of the anapole, as we will see. Unit-cell structure factors for Bragg spots indexed by $(0, 0, l)$ with l odd using axial multipoles described by space group No. 33.151 are

a standard cartoon using dipoles, our fundamental magnetic motifs are block states $\downarrow\downarrow\uparrow\uparrow\downarrow\downarrow$ or staggered states $\downarrow\uparrow\downarrow\uparrow$, with ferromagnetic (α) or antiferromagnetic (β) coupling between chains. Dipoles are conventional (axial) moments or anapoles (Dirac dipole). Likely, Rakhecha *et al.* [30] recorded the first observation by neutron Bragg diffraction of anapoles by way of their contribution to magnetic field-induced patterns gathered on a $C15$ cubic Laves compound UAl_2 . It is well known that the reflection indexed $(2, 2, 2)$ is basis forbidden in such diamondlike structures, and any intensity must arise from a distribution of electrons that violates spatial inversion. Rakhecha *et al.* [30] reported weak basis-forbidden intensities

and confirmed their origin as magnetic by use of neutron polarization analysis. A successful interpretation of the entire diffraction pattern with a correct magnetic space group followed almost four decades later, and it showed that (2, 2, 2)-type reflections are due to anapoles beyond reasonable doubt [31].

Candidates for magnetic motifs in Na_2FeSe_2 studied here belong to 1 of 3 categories defined by a magnetic crystal class and a magnetoelectric property. Magnetic space groups are cataloged in Table I. Our electronic structure factors apply to multipoles of arbitrary rank, moreover, and they are used to predict Bragg diffraction patterns for beams of neutrons or x rays that reveal multipole orders. An inelastic neutron scattering study of ferrous fluoride showed unmissable hybridization of magnons and phonons [27,28]. Vibrations in the electric crystal field modulate the orbital state of the single electron outside the half-filled $3d$ shell, and the mechanism might feature in magnetic excitations in Na_2FeSe_2 .

Likewise, BaFe_2Se_3 with two ladders of dipole moments, space group $Pnm2_1$ (#31) has been used as a makeshift device

to describe local structure in this material [7]. However, if bulk polarization in BaFe_2Se_3 is zero, the parent structure is described by space group $Pnma$ (not $Pnm2_1$), even if somewhere locally in the crystal there are some polar displacements. In fact, magnetic space group C_2c (No. 9.41, polar crystal class $m1'$) used by the authors of Ref. [8] follows if $Pnm2_1$ is substituted for the correct parent structure. The magnetic motif in BaFe_2Se_3 possesses a propagation vector $(\frac{1}{2}, \frac{1}{2}, \frac{1}{2})$ in the parent structure that is equivalent to $(1, 1, -1)_m$ in the monoclinic cell. The first magnetic Bragg spot $(1, 1, 0)_m$ equates to a reflection vector of magnitude $\approx 0.71 \text{ \AA}^{-1}$, or $w \approx 1.14$ in Fig. 4, and all radial integrals in the anapole have significant values.

ACKNOWLEDGMENTS

Figure 3 was prepared by Dr. V. Scagnoli. Professor G. van der Laan commented on the communication in its making and prepared Fig. 4 from calculations he performed.

-
- [1] P. Stüble, S. Peschke, D. Johrendt, and C. Röhr, *J. Solid State Chem.* **258**, 416 (2018).
- [2] B. Pandey, L.-F. Lin, R. Soni, N. Kaushal, J. Herbrych, G. Alvarez, and E. Dagotto, *Phys. Rev B* **102**, 035149 (2020).
- [3] P. J. Hirschfeld, M. M. Korshunov, and I. I. Mazin, *Rep. Prog. Phys.* **74**, 124508 (2011).
- [4] R. M. Fernandes and A. V. Chubukov, *Rep. Prog. Phys.* **80**, 014503 (2017).
- [5] D. Welz and M. Nishi, *Phys. Rev. B* **45**, 9806 (1992).
- [6] R. G. Veliyev, *Semiconductors* **45**, 158 (2011).
- [7] M. Mourigal, Shan Wu, M. B. Stone, J. R. Neilson, J. M. Caron, T. M. McQueen, and C. L. Broholm, *Phys. Rev. Lett.* **115**, 047401 (2015).
- [8] S. W. Lovesey, D. D. Khalyavin, and G. van der Laan, *Phys. Scripta* **91**, 015803 (2016).
- [9] F. Bloch, *Phys. Rev.* **50**, 259 (1936); **51**, 994 (1937).
- [10] J. Schwinger, *Phys. Rev.* **51**, 544 (1937).
- [11] A. Migdal, *Comptes Rendus Acad. Sci. URSS* **20**, 551 (1938).
- [12] G. T. Trammell, *Phys. Rev.* **92**, 1387 (1953).
- [13] D. F. Johnston, *Proc. Phys. Soc.* **88**, 37 (1966).
- [14] D. F. Johnston and D. E. Rimmer, *J. Phys. C Solid State Phys.* **2**, 1151 (1969).
- [15] S. W. Lovesey, *J. Phys. C Solid State Phys.* **2**, 470 (1969).
- [16] S. W. Lovesey, *Theory of Neutron Scattering from Condensed Matter* (Clarendon Press, Oxford, 1987), Vol. 2.
- [17] J. P. Hannon, G. T. Trammell, M. Blume, and D. Gibbs, *Phys. Rev. Lett.* **61**, 1245 (1988); **62**, 2644(E) (1989); J. Luo, G. T. Trammell, and J. P. Hannon, *ibid.* **71**, 287 (1993).
- [18] S. W. Lovesey, *Phys. Scripta* **90**, 108011 (2015).
- [19] *Fifty Years of Neutron Diffraction: The Advent of Neutron Scattering*, edited by G. E. Bacon (Adam Hilger, London, 1987).
- [20] R. D. Cowan, *The Theory of Atomic Structure and Spectra*, (University of California Press, Berkeley, 1981).
- [21] S. W. Lovesey, D. D. Khalyavin and U. Staub, *J. Phys.: Condens. Matter* **27**, 292201 (2015); S. W. Lovesey, and D. D. Khalyavin, *ibid.* **27**, 495601 (2015).
- [22] S. W. Lovesey, E. Balcar, K. S. Knight, and J. Fernández Rodríguez, *Phys. Reports* **411**, 233 (2005).
- [23] V. Scagnoli and S. W. Lovesey, *Phys. Rev. B* **79**, 035111 (2009).
- [24] B. T. Thole, P. Carra, F. Sette, and G. van der Laan, *Phys. Rev. Lett.* **68**, 1943 (1992); P. Carra, B. T. Thole, M. Altarelli, and X. D. Wang, *ibid.* **70**, 694 (1993); P. Carra, H. König, B. T. Thole, and M. Altarelli, *Physica B* **192**, 182 (1993).
- [25] D. H. Templeton and L. K. Templeton, *Acta Crystallogr. A* **36**, 237 (1980); **38**, 62 (1982).
- [26] U. Staub, Y. Bodenthin, C. Piamonteze, M. García-Fernández, V. Scagnoli, M. Garganourakis, S. Koohpayeh, D. Fort, and S. W. Lovesey, *Phys. Rev. B* **80**, 140410(R) (2009).
- [27] B. D. Rainford, J. G. Houmann, and H. J. Guggenheim, 5th IAEA Symp. on Neutron Inelastic Scattering, STI/PUB/308 92-0-030172-X (1972).
- [28] S. W. Lovesey, *J. Phys. C: Solid State Phys.* **7**, 2039 (1974).
- [29] We use the BNS setting of magnetic space groups, see Bilbao Crystallographic server, <http://www.cryst.ehu.es>.
- [30] V. C. Rakhecha, G. H. Lander, A. J. Arko, and R. M. Moon, *J. Appl. Phys.* **52**, 1636 (1981).
- [31] S. W. Lovesey, D. D. Khalyavin, and G. van der Laan, *J. Phys.: Conf. Ser.* **1316**, 012004 (2019).